Macromolecules
ARTICLE

*Macromolecules* **2009**, *42*, 8835–8843 **8835**
DOI: 10.1021/ma9018944

# Hierarchical Self-Assembled Structures from POSS-Containing Block Copolymers Synthesized by Living Anionic Polymerization

**Tomoyasu Hirai,[†,⊥] Melvina Leolukman,[§,⊥] Sangwoo Jin,[‡] Raita Goseki,[†] Yoshihito Ishida,[†] Masa-aki Kakimoto,[†] Teruaki Hayakawa,*[,†] Moonhor Ree,*[,‡] and Padma Gopalan*[,§]**

[†]*Department of Organic and Polymeric Materials, Tokyo Institute of Technology, 2-12-1-S8-36 O-okayama, Meguro-ku, Tokyo 152-8552, Japan,* [‡]*Department of Chemistry, National Research Lab. for Polymer Synthesis and Physics, Pohang Accelerator Laboratory, Center for Electro-Photo Behaviors in Advanced Molecular Systems, BK School of Molecular Science, and Division of Advanced Materials Science, Pohang University of Science and Technology, Pohang 790-784, Republic of Korea, and* [§]*Department of Materials Science and Engineering, University of Wisconsin—Madison, Madison, Wisconsin 53706.* [⊥]*Both authors contributed equally*

*Received August 26, 2009; Revised Manuscript Received October 12, 2009*

ABSTRACT: Two kinds of polyhedral oligomeric silsesquioxane (POSS)-containing block copolymers (BCPs), namely PS-*b*-PMAPOSS and PMMA-*b*-PMAPOSS, were synthesized by living anionic polymerization. A wide range of molecular weights were obtained with a very narrow polydispersity index of less than 1.09. The bulk samples prepared by slow evaporation from a polymer solution in chloroform exhibit well-defined microphase-separated structures with long-range order. Thermal annealing induced hierarchical structures consisting of a smaller length scale ordered crystalline POSS domains within the larger microphase-separated structures. We report detailed structural characterization of these hierarchical structures in bulk and thin films by transmission electron microscopy and grazing incidence wide-angle X-ray scattering (GIWAXS). On the basis of this structural analysis, we propose a model for the formation of an orthorhombic lattice structure through the aggregation of POSS segments which formed a helix-like structure.

## Introduction

The use of block copolymer (BCP) materials in thin-film form to create dense, periodic arrays of small features termed "block copolymer lithography" has inspired the synthesis of a rich array of new BCPs.[1] Some of these BCPs are based on polysytrene-*b*-poly(methyl methacrylate) (PS-*b*-PMMA)[2] where the PMMA block is selectively removed by UV exposure and the patterns are transferred to the underlying silicon substrate using the remaining PS template.[3] There are other examples of organic−organic BCPs which have been examined as candidates for nanofabrication. These include BCPs such as polystyrene-*b*-poly(4-vinylpyridine) (PS-*b*-P4VP),[4] polystyrene-*b*-polylactide (PS-*b*-PLA),[5] and polystyrene-*b*-poly(ethylene oxide) (PS-*b*-PEO).[6] In the case of cylinder forming PS-*b*-PLA film, nanoporous templates are formed by a combination of hydrolytic degradation of PLA and oxygen reactive ion etching. More recently, 10 Tbit/in.[2] ordered cylindrical arrays were fabricated by the self-assembly of Au salt-complexed selectively into the PEO domain of PS-*b*-PEO BCP. The etch selectivity between the blocks can be drastically improved by incorporating Fe- or Si-containing monomers in an organic−inorganic hybrid BCP system. Fe-containing blocks, such as polystyrene-*b*-polyferrocenylsilane (PS-*b*-PFS), have been explored extensively as etch masks.[7,8] Silicon-containing BCPs have similar etching behavior as metal-containing polymers and are completely compatible with integrated circuit process.[9] Recently, polystyrene-*b*-polydimethylsiloxane (PS-*b*-PDMS) BCPs which form in-plane cylinders have been adapted as templates.[10] The significantly lower surface tension of the PDMS block compared to PS poses processing challenges during pattern transfer.

It is highly desirable to explore other morphologies such as vertically oriented lamellae or cylinders which have direct connectivity to the underlying substrate for pattern transfer, while retaining the high etch selectivity between the two blocks and the ability to access sub-10 nm feature sizes.[11] To meet these requirements, we have focused our efforts on polyhedral oligomeric silsesquioxane (POSS)-containing BCPs. POSS molecules are known to form nanometer size semicrystalline or crystalline domains, which are thermally and physically robust and are converted to silica upon exposure to oxygen plasma.[12] Random copolymers containing POSS units have been synthesized by a number of methods including conventional free radical polymerization[13] and ring-opening metathesis polymerization.[14] These random copolymers exhibit lamella-like POSS aggregates which lack long-range order.[15]

To achieve long-range order, it is important to examine block copolymers instead of random copolymers. Pyun et al. have demonstrated the atom transfer radical polymerization (ATRP) of methacrylate-functionalized POSS. In this case, the degree of polymerization (DP) was less than 15 since the steric hindrance of POSS inhibits the formation of copper(I) complex with chain ends.[16] In a previous work, we demonstrated that hydrosilylation of polystyrene-*b*-poly(1,2-*ran*-3,4-isoprene) [PS-*b*-PI] with hydrido-heptacyclopentyl-substituted POSS results in the incorporation of POSS in the PI domain (PS-*b*-PIPOSS).[17] As expected, the postfunctionalization reaction did not incorporate POSS in all the PI units. In both of these cases while microphase separation

*Corresponding authors: Tel +81-3-5734-2421 (T.H.), 608-265-4258 (P.G.), +82-54-279-2120 (M.R.); Fax +81-3-5734-2875 (T.H.), 608-262-8353 (P.G.), +82-54-279-3399 (R.M.); e-mail hayakawa.t.ac@m.titech.ac.jp (T.H.), ree@postech.edu (M.R.), pgopalan@wisc.edu (P.G.).


Published on Web 10/29/2009

was observed, however, smaller length scale ordering due to POSS was not observed. The formation of semicrystalline or crystalline POSS nanostructures within the microphase-separated domains could offer potential advantages in improving the line edge roughness of the resulting structures as the intermaterial dividing surface is likely to be ultrathin due to the crystalline POSS units which are a few nanometers in size.

Recently, we reported the living anionic polymerization route to POSS-containing block copolymers, namely PS-*b*-PMAPOSS and PMMA-*b*-PMAPOSS, resulting in the formation of well-defined self-assembled hierarchical nanostructures.[18] The narrow polydispersity index (PDI) and high DP achievable by anionic polymerization route drives the formation of these hierarchical nanostructures. In a subsequent publication, we have shown that these two (lamella and cylinder forming) BCPs show excellent self-assembling abilities in thin film by a simple solvent annealing process on unmodified substrates. The resulting feature sizes in the case of cylindrical morphology were as small as 10 nm.[19]

Here, we report the details of the living anionic polymerization of methacrylate-functionalized POSS and the synthesis of its block copolymers with both PS and PMMA resulting in spherical, cylindrical, and lamellar morphologies. We report detailed structural characterization of these hierarchical structures in bulk and thin films by transmission electron microscopy and synchrotron X-ray scattering.

## Experimental Section

**Material.** *Sec*-Butyllithium (*sec*-BuLi) was purchased from Aldrich and Kanto Chemical Co., Inc. Other chemicals were purchased from Aldrich. Tetrahydrofuran (THF) was freshly distilled from sodium/benzophenone (deep purple color) under nitrogen after refluxing for at least 3 h. Styrene was purified first by washing with sodium hydroxide (NaOH) solution to remove inhibitor before stirring with calcium hydride ($CaH_2$) for 24 h and then distilling under vacuum. Methyl methacrylate (MMA) was stirred with $CaH_2$ for 24 h and then distilled under vacuum. The purified monomers were stored in an argon atmosphere. Prior to use, the monomers were treated with a small amount of di-*n*-butylmagnesium (styrene) and triethylaluminum (MMA) and redistilled. 1,1-Diphenylethylene (DPE) was distilled over *n*-butyllithium. 3-(3,5,7,9,11,13,15-Heptaisobutylpentacyclo-[9.5.1.$^{3,9}$1$^{5,15}$1$^{7,13}$]octasiloxan-1-yl)propyl methacrylate (MAPOSS) was recrystallized from methanol (MeOH) and dried in a vacuum oven at 60 °C for 24 h. Lithium chloride (LiCl) was baked under vacuum at 180 °C for 24 h. *sec*-BuLi (1.4 M solution in cyclohexane and 1.07 M solution in cyclohexane and hexane), MeOH, di-*n*-butylmagnesium, triethylaluminum, NaOH, and $CaH_2$ were used as received.

**Instrumentation and Characterization.** *Methods*. For transmission electron microscopy (TEM) measurements, bulk samples were embedded in epoxy and cured at 70 °C for 24 h. The embedded samples were then microtomed by a Diatome diamond knife at room temperature into a preset thickness of 70 nm using a Reichert-Jung Ultracut E Microtome. The sections were picked up by the TEM grids and viewed directly with bright field Phillip CM 120 TEM at 80 kV accelerating voltage (Medical School Electron Microscope Facility at University of Wisconsin—Madison). POSS appeared darker due to its higher electron density compared to PS or PMMA. Transmission wide- and small-angle X-ray scattering (TWAXS and TSAXS) measurements for the bulk samples were performed on the Sector 8-ID-E beamline at Advanced Photon Source at Argonne National Laboratory. Monochromatic X-ray beams of 7.35 keV ($\lambda$ = 0.168 68 nm: $\lambda$, wavelength) were used.

Grazing incidence wide-angle X-ray scattering (GIWAXS) measurements for PMMA-*b*-PMAPOSS thin films spin-coated on Si wafers were carried out at the 4C2 beamline at Pohang

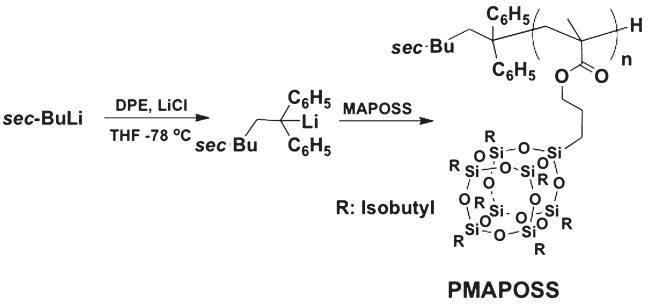


**Figure 1.** Synthesis of PMAPOSS homopolymer by living anionic polymerization.

**Table 1. Molecular Weight and Polydispersity of PMAPOSS as a Function of the Monomer/Initiator Ratio**

| monomer/ initiator ratio | $M_n$(calcd)[a] (g/mol) | $M_n$(MALS)[b] (g/mol) | $M_n$(SEC)[c] (g/mol) | PDI[c] |
|---|---|---|---|---|
| 19.6 | 18 500 | 15 500 | 7 800 | 1.03 |
| 77.8 | 73 400 | 69 900 | 22 200 | 1.04 |
| 98.1 | 92 500 | 93 400 | 29 000 | 1.04 |

[a] Molecular weights calculated from the monomer/ initiator ratios. [b] Molecular weights measured by multiangle laser light scattering. [c] Molecular weights measured by SEC calibrated against PS linear standard.

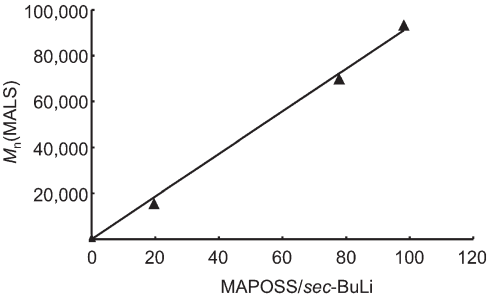


**Figure 2.** $M_n$(MALS) of PMAPOSS as a function of monomer (MAPOSS)/initiator (*sec*-BuLi) ratio.

Accelerator Laboratory.[20] A monochromatized X-ray radiation source of 8.979 keV ($\lambda$ = 0.138 nm) and a two-dimensional charge-coupled device (2D CCD) detector (Roper Scientific, Trenton, NJ) were used. The sample-to-detector distance was 124.2 mm. A set of aluminum foil strips was employed as semitransparent beam stops because the intensity of the specular reflection from the substrate is much stronger than the intensity of GIWAXS near the critical angle. Samples were mounted on a homemade *z*-axis goniometer equipped with a vacuum chamber. The incidence angle $\alpha_i$ of X-ray beam was set in the range 0.16°−0.20°, which is between the critical angle of the PMMA-*b*-PMAPOSS thin film and the silicon substrate ($\alpha_{c,f}$ and $\alpha_{c,s}$). Scattering angles were corrected by the positions of X-ray beams reflected from the silicon substrate interface with changing incidence angle $\alpha_i$ and by a precalibrated silver behenate powder (TCI, Japan). Data were typically collected for 30 s.

$^1$H (300 MHz), $^{13}$C (75 MHz), and $^{29}$Si (59.4 MHz) NMR spectra were recorded in $CDCl_3$ on a JEOL JNM-AL 300 spectrometer at 300, 75, and 59.4 MHz, respectively. IR spectra were recorded on a JASCO FT/IR-460 Plus spectrophotometer. Size exclusion chromatography (SEC) measurements were carried out using Shodex GPC-101 with two columns (Shodex KF-802 and Shodex KF-806M), detectors Shoedex RI-71 (relative molecular weight), and miniDAWN Tristar (absolute molecular weight). THF was used as an eluent with 1 mL min$^{-1}$ flow rate at 40 °C. Relative molecular weights are quoted with monodisperse polystyrenes as standard. Tapping mode atomic force microscopy (AFM) measurements were performed on Seiko

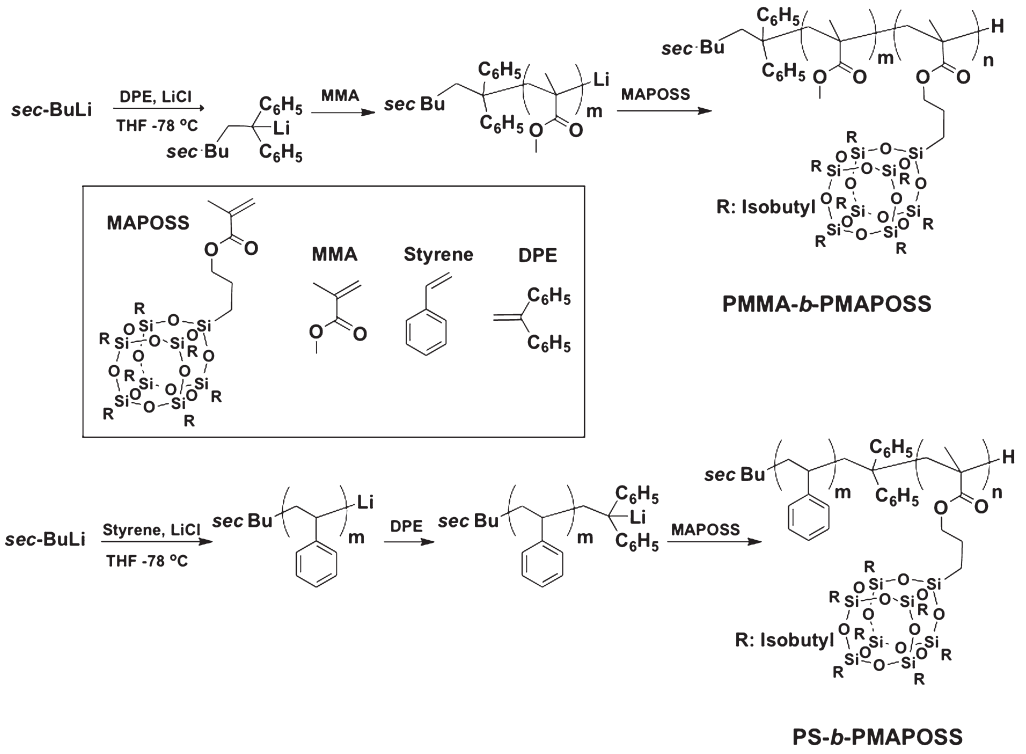


**Figure 3.** Synthesis of block copolymers PMMA-*b*-PMAPOSS and PS-*b*-PMAPOSS by living anionic polymerization.

**Table 2. Summary of Molecular Weight, Molecular Weight Distribution and Morphology of PMMA-*b*-PMAPOSS BCPs**

| PMMA-*b*-PMAPOSS[a] | $M_n$(SEC)[b] (g/mol) | $M_n$(MALS)[c] (g/mol) | mol %[d] | wt %[d] | vol %[e] | PDI[b] | morphology[f] |
|---|---|---|---|---|---|---|---|
| $PMMA_{41}$-*b*-$PMAPOSS_{29}$ | 31 300 | 80 660 | 59/41 | 13/87 | 13/87 | 1.03 | PMMA cylinder |
| $PMMA_{52}$-*b*-$PMAPOSS_{18}$ | 37 400 | 105 700 | 58/42 | 13/87 | 13/87 | 1.08 | PMMA cylinder |
| $PMMA_{35}$-*b*-$PMAPOSS_{15}$ | 17 400 | 36 400 | 71/29 | 20/80 | 20/80 | 1.04 | PMMA cylinder |
| $PMMA_{52}$-*b*-$PMAPOSS_{18}$ | 22 500 | 49 120 | 73/27 | 23/77 | 23/77 | 1.05 | PMMA cylinder |
| $PMMA_{270}$-*b*-$PMAPOSS_{28}$ | 53 000 | 94 000 | 91/9 | 51/49 | 51/49 | 1.06 | lamella |
| $PMMA_{262}$-*b*-$PMAPOSS_{23}$ | 47 700 | 75 400 | 92/8 | 55/45 | 55/44 | 1.08 | lamella |
| $PMMA_{428}$-*b*-$PMAPOSS_{15}$ | 57 100 | 86 700 | 97/3 | 75/25 | 75/25 | 1.08 | lamella |
| $PMMA_{450}$-*b*-$PMAPOSS_{7}$ | 51 700 | 75 800 | 98/2 | 87/13 | 87/13 | 1.06 | POSS sphere |

[a] The numbers refer to the final composition determined by SEC calibrated against PS linear standard and integrations from $^1$H NMR spectra. [b] Molecular weights measured by SEC calibrated against PS linear standard. [c] Molecular weights measured by multiangle laser light scattering. [d] Determined by $^1$H NMR spectra. [e] Determined by density gradient column, integration from $^1$H NMR spectra, and SEC measurement calibrated against as PS linear standard. [f] Observed by TEM.

model SPA-400. Polymer density was estimated by homemade density gradient column using KI aqueous solution at 25 °C, 1-bromododecane (1.038 g/cm$^3$), 1-bromoundecane (1.054 g/cm$^3$), diphenyl ether (1.073 g/cm$^3$), chlorobenzene (1.107 g/cm$^3$), ethyl 4-fluorobenzenoate (1.146 g/cm$^3$), 1-bromohexane (1.176 g/cm$^3$), nitrobenzene (1.196 g/cm$^3$), and ethyl 6-bromohexanoate (1.254 g/cm$^3$) as a references. PMMA-*b*-PMAPOSS thin films were prepared by spin-coating 5.0 (w/w) polymer solution in cyclopentanone onto silicon wafer with native oxide layer at 4000 rpm for 60 s. Prior to film casting, silicon (100) substrates were cleaned in a piranha solution, a mixture of $H_2O_2$ (30%)/$H_2SO_4$ (70%) (v/v) at 110 °C for 2 h, rinsed with distilled water, and dried in a stream of nitrogen.

*Synthesis of PMAPOSS Homopolymers by Living Anionic Polymerization.* 40 mL of THF was transferred to a glass reactor containing 15 mg of dry LiCl (0.36 mmol), and the glass reactor was cooled to −78 °C. After 5 min, *sec*-BuLi was added until the color changed to slight yellow. The reactor was removed from the cooling bath and allowed to reach room temperature, upon which the solution became colorless. The reactor was cooled back to −78 °C, and 0.025 mL of 1.07 M *sec*-BuLi solution in hexane/cyclohexane (0.027 mmol) was added. After 5 min, 0.025 mL of DPE (0.14 mmol) was added to the reactor, resulting in a deep red color. In an ampule, 2.00 g of MAPOSS (2.1 mmol) was dissolved in THF (4.0 mL). After 30 min, 2.00 g of MAPOSS (2.1 mmol), predissolved in THF (4.0 mL), was transferred from the monomer reservoir to the polymerization flask via cannula with vigorous stirring. The solution changes from deep red to colorless. After 6 h at −78 °C, excess of MeOH was added to the reactor obtain the proton-terminated polymer. The polymer was then precipitated into MeOH, filtered, and dried under vacuum at 80 °C for 24 h, resulting in 1.71 g of polymer. Yield: 85%. For the final polymer, SEC gives $M_n$(SEC) of 22 200 g/mol and polydispersity ($M_w/M_n$) of 1.04. IR (KBr, $\nu$, cm$^{-1}$): 2995, 2928, 2908, 2871, 1734, 1465, 1402, 1383, 1366, 1332, 1230, 1168, 1107, 1037. $^1$H NMR (300 MHz, $CDCl_3$, $\delta$, ppm): 3.81 (br, −O−C$H_2$), 1.86−1.54 (m, isobutyl −C$H$, main chain −C$H_2$), 0.95−0.93 (br, isobutyl −C(C$H_3$)$_2$), 0.59 (br, −SiC$H_2$). $^{13}$C NMR (75 MHz, $CDCl_3$, $\delta$, ppm): 176.9, 67.2, 45.2, 26.0, 25.8, 25.7, 25.5, 24.0, 23.8, 22.5, 22.4, 21.4, 8.4. $^{29}$Si NMR (59.4 MHz, $CDCl_3$, $\delta$, ppm): −67.6, −67.9.

*Synthesis of PMMA-b-PMAPOSS by Living Anionic Polymerization.* 40 mL of THF was transferred to a glass reactor containing 15 mg of dry LiCl (0.36 mmol), and the reactor was cooled to −78 °C. Five minutes later, *sec*-BuLi was added until color changed to light yellow. The reactor was removed from the cooling bath and allowed to reach room temperature upon which the solution becomes colorless. The reactor was cooled

**Table 3. Summary of Molecular Weight, Molecular Weight Distribution and Morphology of PS-*b*-PMAPOSS BCPs**

| PS-*b*-PMAPOSS[a] | $M_n$(SEC)[b] (g/mol) | $M_n$(MALS)[c] (g/mol) | mol %[d] | wt %[d] | vol %[e] | PDI[e] | morphology[f] |
|---|---|---|---|---|---|---|---|
| $PS_{69}$-*b*-$PMAPOSS_{47}$ | 51 300 | 138 000 | 60/40 | 14/86 | 15/85 | 1.09 | PS cylinder |
| $PS_{51}$-*b*-$PMAPOSS_{32}$ | 35 500 | 86 900 | 61/39 | 15/85 | 17/83 | 1.05 | PS cylinder |
| $PS_{65}$-*b*-$PMAPOSS_{18}$ | 24 100 | 47 900 | 78/22 | 28/72 | 30/70 | 1.05 | PS cylinder |
| $PS_{52}$-*b*-$PMAPOSS_{9}$ | 13 400 | 20 390 | 86/14 | 40/60 | 42/58 | 1.07 | PS cylinder |
| $PS_{206}$-*b*-$PMAPOSS_{28}$ | 47 500 | 91 800 | 88/12 | 45/55 | 47/53 | 1.09 | lamella |
| $PS_{266}$-*b*-$PMAPOSS_{20}$ | 47 000 | 67 500 | 93/7 | 59/41 | 63/37 | 1.05 | lamella |
| $PS_{183}$-*b*-$PMAPOSS_{6}$ | 25 000 | 29 100 | 97/3 | 76/24 | 77/23 | 1.04 | lamella |
| $PS_{394}$-*b*-$PMAPOSS_{4}$ | 43 400 | 48 100 | 99/1 | 92/8 | 93/7 | 1.03 | POSS sphere |
| $PS_{587}$-*b*-$PMAPOSS_{4}$ | 64 900 | 71 000 | 99/1 | 94/6 | 96/4 | 1.07 | POSS sphere |

[a] The numbers refer to the final composition determined by SEC calibrated against PS linear standard and integrations from $^1$H NMR spectra. [b] Molecular weights measured by SEC calibrated against PS linear standard. [c] Molecular weights measured by multiangle laser light scattering. [d] Determined by $^1$H NMR spectra. [e] Determined by density gradient column, integration from $^1$H NMR spectra, and SEC measurement calibrated against as PS linear standard. [f] Observed by TEM.

back to −78 °C, and 0.025 mL of 1.07 M *sec*-BuLi solution in hexane/cyclohexane (0.027 mmol) was added. After an additional 5 min, 0.025 mL of DPE (0.14 mmol) was added to the reactor, resulting in a deep red color. After 30 min, 0.25 mL of MMA (2.3 mmol) was transferred from the monomer reservoir to the polymerization flask via cannula with vigorous stirring. The deep red color changes to light yellow. In a second ampule, 1.90 g of MAPOSS (2.0 mmol) was dissolved in THF (4.0 mL). After 30 min, the MAPOSS solution was transferred to the polymerization flask via cannula. After 9 h at −78 °C, an excess of methanol was added to the reactor in order to prepare the proton-terminated diblock copolymer. The polymer was then precipitated into MeOH, filtered, and dried under vacuum at 80 °C for 24 h, resulting in 1.68 g of polymer. Yield: 79%. For final block copolymer, SEC gives $M_n$(SEC) of 31 300 g/mol and polydispersity ($M_w/M_n$) of 1.03. IR (KBr, $\nu$, cm$^{-1}$): 2995, 2953, 1732, 1484, 1449, 1438, 1388, 1366, 1333, 1272, 1241, 1193, 1148. $^1$H NMR (300 MHz, $CDCl_3$, $\delta$, ppm): 3.81 (br, −OC$H_2$, PMAPOSS), 3.58 (br, −OC$H_3$, PMMA), 1.86−1.54 (m, isobutyl −C*H*, main chain −C$H_2$, PMAPOSS, PMMA), 0.95−0.93 (br, isobutyl −C(C$H_3$)$_2$, PMAPOSS), 0.84 (m, α−C$H_3$, PMMA), 0.59 (br, −SiC$H_2$, PMAPOSS). $^{13}$C NMR (75 MHz, $CDCl_3$, $\delta$, ppm): 178.0, 177.7, 176.9, 66.8, 54.1, 52.4, 51.7, 44.8, 44.5, 44.4, 25.7, 25.6, 23.7, 22.4, 22.3, 18.6, 16.5, 8.3. $^{29}$Si NMR (59.4 MHz, $CDCl_3$, $\delta$, ppm): −67.6, −67.9.

*Synthesis of PS-b-PMAPOSS by Living Anionic Polymerization.* 40 mL of THF was transferred to a glass reactor containing 15 mg of dry LiCl (0.36 mmol), and the reactor was cooled to −78 °C. Five minutes later *sec*-BuLi was added until color changed to light yellow. The reactor was removed from the cooling bath and allowed to reach room temperature, upon which the solution became colorless. The reactor was cooled back to −78 °C, and 0.025 mL of 1.4 M *sec*-BuLi solution in cyclohexane (0.035 mmol) was added after 5 min. After an additional 5 min, 1.9 mL of styrene (16 mmol) was transferred from the monomer reservoir to the polymerization flask via cannula with vigorous stirring. A bright orange-yellow color soon developed. After 10 min, 0.025 mL of DPE (0.14 mmol) was added to the reactor, resulting in a deep red color. In a second ampule, 1.90 g of MAPOSS (2.0 mmol) was dissolved in THF (4 mL). After 30 min, the MAPOSS solution was transferred to the polymerization flask via cannula. The deep red color changed to light yellow. After 9 h at −78 °C, an excess of methanol was added to the reactor in order to prepare the proton-terminated diblock copolymer. The polymer was then precipitated into MeOH, filtered, and dried under vacuum at 80 °C for 24 h, resulting in 2.90 g of polymer. Yield: 80%. For final block copolymer, SEC gives $M_n$(SEC) of 47 500 g/mol and polydispersity ($M_w/M_n$) of 1.09. IR (KBr, $\nu$, cm$^{-1}$): 3083, 3060, 3026, 3001, 2953, 2924, 2871, 2850, 1942, 1735, 1602, 1493, 1452, 1230, 1169, 1108, 1029. $^1$H NMR (300 MHz, $CDCl_3$, $\delta$, ppm): 7.06 (m, aromatic, PS), 6.56 (m, aromatic, PS), 3.82 (m, −O−C$H_2$, PMAPOSS), 2.12−1.84 (m, main chain −C$H_2$, −C*H*, (PMAPOSS, PS), isobutyl −C*H*, (PMAPOSS)), 1.41 (m, main chain −C$H_2$, PS), 0.97−0.95 (br, isobutyl −C(C$H_3$)$_2$, PMAPOSS), 0.60 (br, −SiC$H_2$, PMAPOSS). $^{13}$C NMR (75 MHz, $CDCl_3$, $\delta$, ppm): 176.8, 146.1, 145.7, 145.3, 145.1, 128.2, 128.0, 127.9, 127.6, 127.4, 127.3, 125.6, 125.5, 67.2, 43.8, 40.3, 25.7, 25.6, 23.8, 22.5, 22.4, 8.6. $^{29}$Si NMR (59.4 MHz, $CDCl_3$, $\delta$, ppm): −67.5, −67.8.

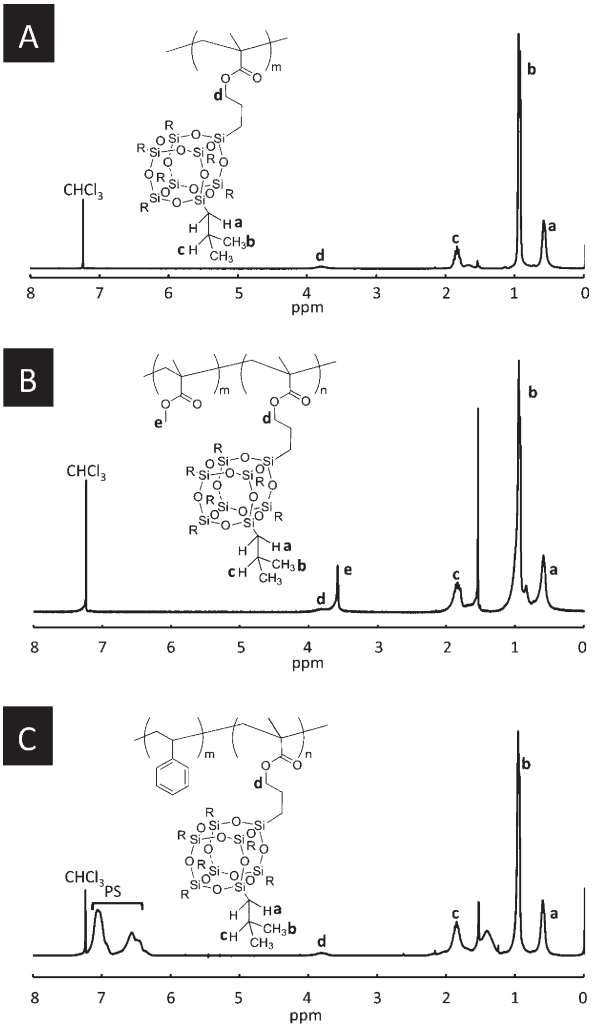


**Figure 4.** $^1$H NMR spectra of (A) PMAPOSS homopolymer, (B) PMMA-*b*-PMAPOSS, and (C) PS-*b*-PMAPOSS in $CDCl_3$.

## Results and Discussion

**Synthesis.** Attempts to polymerize MAPOSS using *sec*-BuLi initiator even at low temperature were unsuccessful as

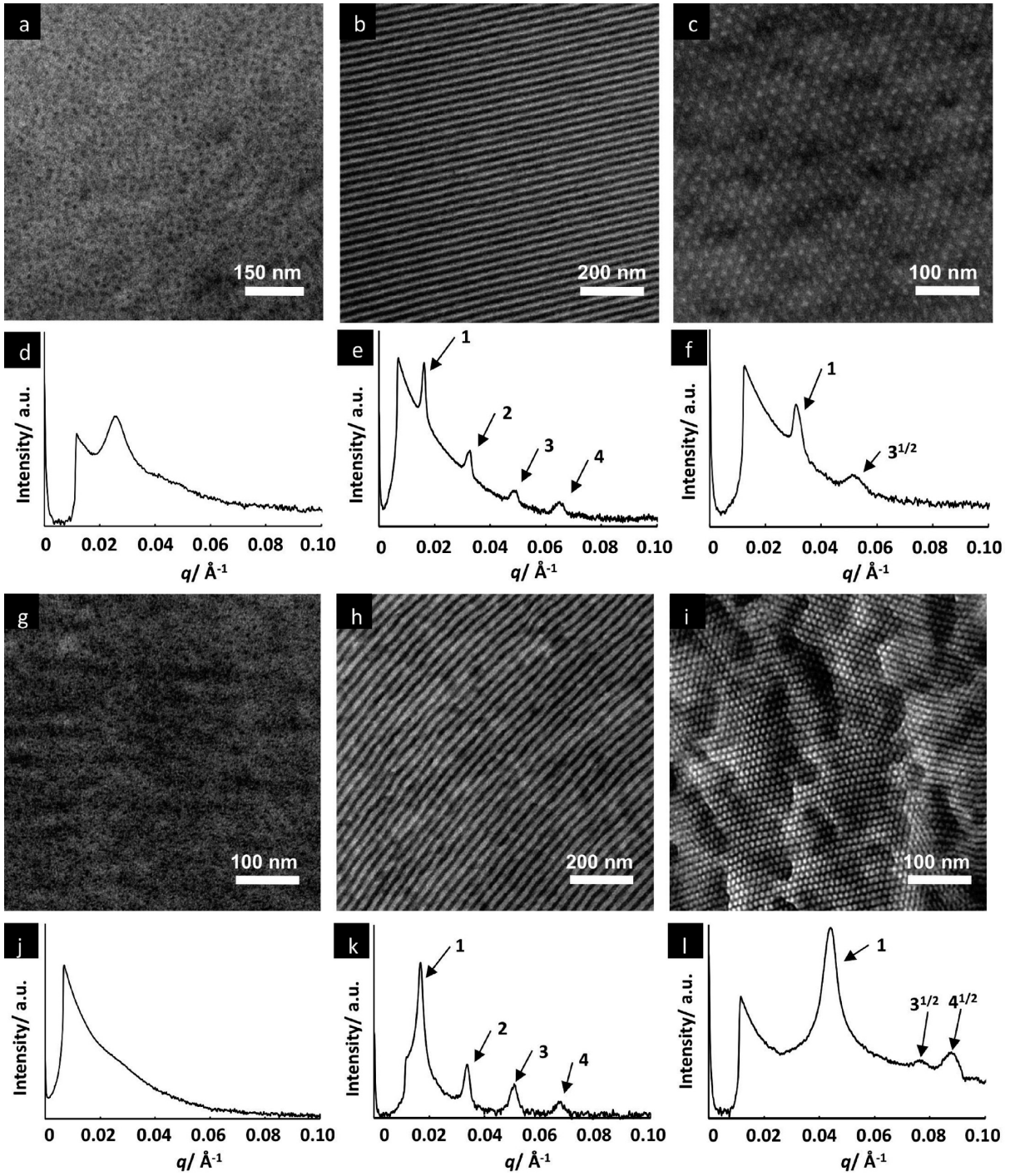


**Figure 5.** TEM and TSAXS profiles of (a, d) $PMMA_{450}$-*b*-$PMAPOSS_7$, (b, e) $PMMA_{262}$-*b*-$PMAPOSS_{23}$, (c, f) $PMMA_{52}$-*b*-$PMAPOSS_{18}$, (g, j) $PS_{587}$-*b*-$PMAPOSS_4$, (h, k) $PS_{266}$-*b*-$PMAPOSS_{20}$, and (i, l) $PS_{52}$-*b*-$PMAPOSS_9$.

the high reactivity of the *sec*-BuLi resulted in significant side reactions by attacking the carbonyl groups in MAPOSS. It is known from the literature in living anionic polymerization of methacrylates that the reactivity of initiators such as BuLi can be inhibited by using excess of LiCl and 1, 1-diphenylethylene (DPE).[21] In fact, this approach works quite well for MAPOSS. PMAPOSS homopolymers were synthesized by living anionic polymerization using *sec*-BuLi initiator in the presence excess of LiCl and DPE at −78 °C for 6 h (Figure 1). Quantitative conversions can be obtained in 6 h as monitored by the $^1$H NMR spectrum. Table 1 shows the relative molecular weight $M_n$(SEC) against PS standards, absolute molecular weight $M_n$(MALS), and polydispersity (PDI) of PMAPOSS as measured by SEC as a function of monomer/initiator ratio. As expected the $M_n$(MALS) is 2−3 times higher than $M_n$(SEC). The compact cage structure of PMAPOSS compared to PS explains the higher absolute molecular weights.[22] Figure 2 shows the variation in $M_n$(MALS) as a function of monomer/initiator ratio. The linear increase in $M_n$(MALS) with the monomer/initiator ratio along with the narrow PDI ( < 1.04) confirms the living nature of the polymerization. In these set of experiments a DP (determined from $M_n$(SEC)) as high as 30 could be obtained for the PMAPOSS, which is 2 times higher than those reported in the literature for block copolymers made by ATRP.[16] It should be noted that even higher DP's should be possible by the anionic route. The

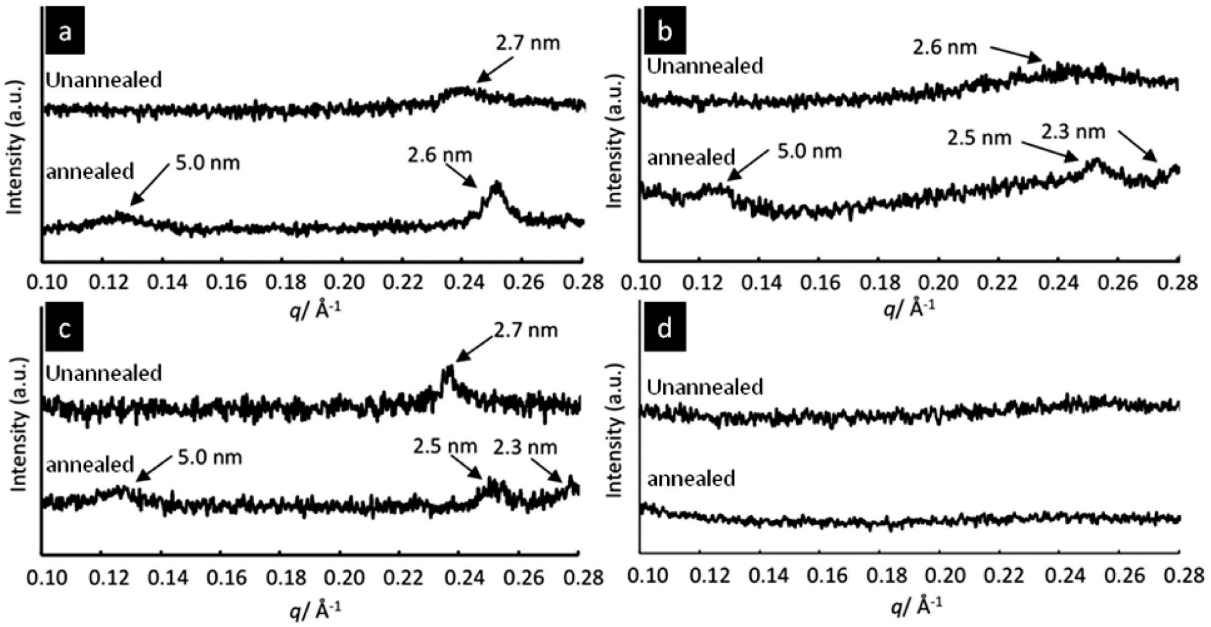


**Figure 6.** TWAXS profiles of unannealed and annealed (a) $PMMA_{262}$-*b*-$PMAPOSS_{23}$, (b) $PMMA_{52}$-*b*-$PMAPOSS_{18}$, (c) $PS_{267}$-*b*-$PMAPOSS_{20}$, and (d) $PS_{52}$-*b*-$PMAPOSS_{9}$.

higher DP can be attributed to the very low activation energy for the propagation of the anion, while the activation of the radical can be inhibited by the bulky POSS.

Using these optimized conditions, two sets of BCPs, namely PMMA-*b*-PMAPOSS and PS-*b*-PMAPOSS, were synthesized with varying volume fraction of each block (Figure 3). The first block consisted of PMMA or PS followed by PMAPOSS as the second block. The polymerization results are listed in Table 2 (PMMA-*b*-PMAPOSS) and Table 3 (PS-*b*-PMAPOSS). The chemical compositions of the BCPs were characterized by $^{1}H$, $^{13}C$, $^{29}Si$ NMR, and IR spectra. The $M_n$(SEC) and $M_n$(MALS) of PMMA-*b*-PMAPOSS and PS-*b*-PMAPOSS were measured by SEC. Figure 4A−C shows representative $^{1}H$ NMR spectra of PMAPOSS homopolymer, PMMA-*b*-PMAPOSS, and PS-*b*-PMAPOSS, respectively. The $^{1}H$ NMR spectra of PMAPOSS show the methylene protons of $-SiCH_2$ from the POSS cage appearing at 0.59 ppm (Figure 4A-a). In the case of PMMA-*b*-PMAPOSS, $-OCH_3$ groups of the PMMA block appear at 3.58 ppm (Figure 4B-e). For PS-*b*-PMAPOSS, the phenyl protons from the PS block appear at 7.06 and 6.56 ppm (Figure 4C-PS). Hence, the compositions of PMMA-*b*-PMAPOSS and PS-*b*-PMAPOSS were ascertained by using the integration ratio's from the $^{1}H$ NMR spectrum of methoxy protons for PMMA or phenyl protons for PS and comparing with the integration of methylene protons from the POSS cage along with the $M_n$(SEC) values. As the number of the POSS segments increases, the difference between $M_n$(MALS) and $M_n$(SEC) becomes larger.

**Bulk Morphological Characterization.** For bulk morphology characterization, it is important to know the volume fraction of each block. The density of PMAPOSS was measured using a density gradient column. The density of PMAPOSS was found to be 1.14 g/cm$^3$ at 25 °C. Using polystyrene density of 1.05 g/cm$^3$ and PMMA density of 1.15 g/cm$^3$ in combination with the $^{1}H$ NMR data, the volume ratios for each block was determined (Tables 2 and 3). Bulk samples of the two kinds of POSS-containing BCPs were prepared by slow evaporation from chloroform solution and characterized by TEM and TSAXS. In the TEM measurements, all samples were imaged without staining as the higher mass contrast of the POSS-containing block compared to PS and PMMA blocks results in PMAPOSS domains appearing as darker regions and either PS or PMMA domains appearing as brighter regions.

Figure 5 shows TEM and TSAXS results of PMMA-*b*-PMAPOSS (a−f) and PS-*b*-PMAPOSS (g−l) BCPs. The TEM images of $PMMA_{450}$-*b*-$PMAPOSS_7$ and $PS_{587}$-*b*-$PMAPOSS_4$ with a PMAPOSS volume fraction of 13% and 4%, respectively, show spherical PMAPOSS morphologies (Figure 5a,g). The scattering profile of the $PMMA_{450}$-*b*-$PMAPOSS_7$ shows a first-order diffraction peak and a broad second-order diffraction peak (Figure 5d), while that of $PS_{587}$-*b*-$PMAPOSS_4$ reveals only a broad first-order diffraction peak (Figure 5j). From the TEM and TSAXS data, the spheres were estimated to have an average diameter of 10 nm and a mean interdistance of 24 nm for the $PMMA_{450}$-*b*-$PMAPOSS_7$ and an average diameter of 6 nm and a mean interdistance of 14 nm for the $PS_{587}$-*b*-$PMAPOSS_4$ sample. These results show that while $PMMA_{450}$-*b*-$PMAPOSS_7$ and $PS_{587}$-*b*-$PMAPOSS_4$ can phase separate into PMAPOSS spheres with a diameter of 6−10 nm, they lack long-range order.

In contrast, well-defined lamellar structures were observed for the $PMMA_{262}$-*b*-$PMAPOSS_{23}$ and $PS_{266}$-*b*-$PMAPOSS_{20}$ with PMAPOSS volume fractions of 44% and 37%, respectively (Figure 5b,h). The scattering profiles show up to fourth-order diffraction peaks with a characteristic ratio of 1:2:3:4, which can be assigned to the (001), (002), (003), and (004) plane, indicating lamellar morphologies (Figure 5e, k).[18] The lamellar *d*-spacing was 38.7 and 37.3 nm for the $PMMA_{262}$-*b*-$PMAPOSS_{23}$ and $PS_{266}$-*b*-$PMAPOSS_{20}$, respectively, which is in good agreement with observed values from the TEM.

For the $PMMA_{52}$-*b*-$PMAPOSS_{18}$ and $PS_{52}$-*b*-$PMAPOSS_9$ with PMAPOSS volume fraction of 77% and 58%, respectively (Figure 5c,i), cylindrical morphology was observed. The TEM images show a hexagonally packed PS or PMMA cylinder (HEX) structure in a PMAPOSS matrix. These results are supported by X-ray observations which show diffraction peaks with a ratio of 1:$\sqrt{3}$ for

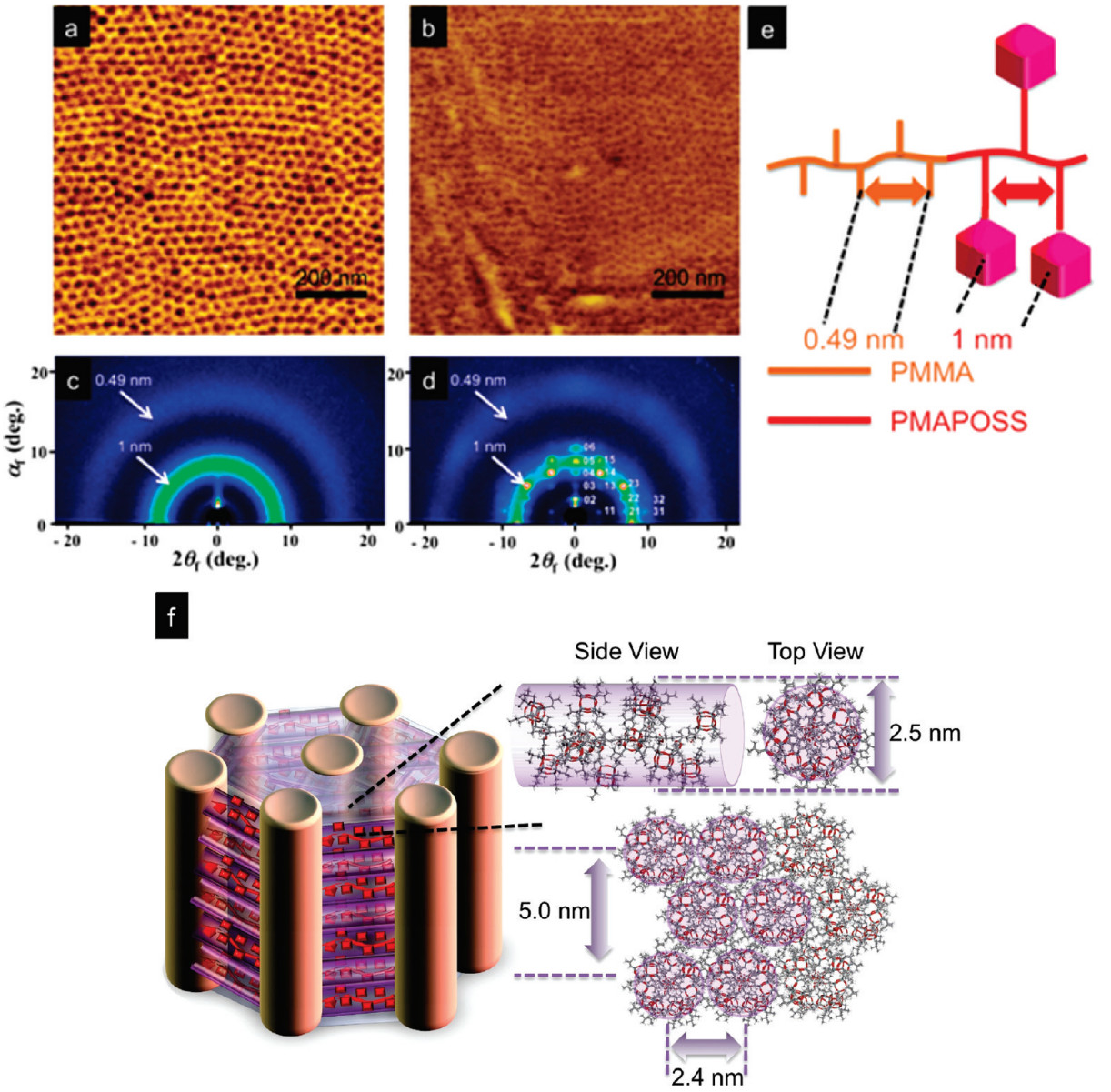


**Figure 7.** AFM phase images and 2D GIWAXS patterns of $PMMA_{41}$-*b*-$PMAPOSS_{29}$ (a, c) $CS_2$ solvent annealing for 10 h, (b, d) thermal annealing at 190 °C for 6 h after solvent annealing, (e) schematic illustration of the relevant length scales in PMMA-*b*-PMAPOSS BCP, and (f) representation of the morphology of thermally annealed $PMMA_{41}$-*b*-$PMAPOSS_{29}$, consisting of PMMA cylinders in a PMAPOSS matrix, where the PMAPOSS segments assume a helix-like structure and the helices are further arranged in an orthorhombic lattice structure.

$PMMA_{52}$-*b*-$PMAPOSS_{18}$ and 1:$\sqrt{3}$:2 for the $PS_{52}$-*b*-$PMAPOSS_9$ sample (Figure 5f,l), which is characteristic of a cylindrical morphology. These peaks are assigned as the diffractions of the (001), (011), and (002) planes, respectively. The distance between the cylinders was found to be 20.4 and 14.3 nm for the $PMMA_{52}$-*b*-$PMAPOSS_{18}$ and $PS_{52}$-*b*-$PMAPOSS_9$, respectively. The diameter of the cylinders was found to be 9.1 nm for $PMMA_{52}$-*b*-$PMAPOSS_{18}$ and 9.5 nm for $PS_{52}$-*b*-$PMAPOSS_9$.

**Effect of Thermal Annealing on Bulk Samples: Formation of Hierarchical Structures.** Lamella ($PMMA_{262}$-*b*-$PMAPOSS_{23}$ and $PS_{266}$-*b*-$PMAPOSS_{20}$) and cylinder ($PMMA_{52}$-*b*-$PMAPOSS_{18}$ and $PS_{52}$-*b*-$PMAPOSS_9$) forming bulk samples were annealed at 190 °C for 24 h to examine any morphological changes. TWAXS studies were conducted to see whether the POSS cages were organized within the phase-separated structure. The unannealed $PMMA_{52}$-*b*-$PMAPOSS_{18}$ sample shows a weak diffraction peak in the high $q$ region corresponding to a $d$-spacing of 2.6−2.7 nm, whereas for $PS_{52}$-*b*-$PMAPOSS_9$ this peak is not visible (Figure 6b,d). Upon annealing the $PMMA_{52}$-*b*-$PMAPOSS_{18}$ sample, diffraction peaks corresponding to a $d$-spacing of 5.0, 2.5, and 2.3 nm emerge, indicating the aggregation of POSS units within the majority domain in the cylinder forming BCP. Thermal annealing did not result in additional diffraction peaks for the $PS_{52}$-*b*-$PMAPOSS_9$ BCP in the scattering profile, suggesting that the short length of the PMAPOSS block is insufficient to drive the formation of hierarchical structures. Similar results indicating aggregation of POSS units within a phase-separated domain were observed upon annealing both $PMMA_{262}$-*b*-$PMAPOSS_{23}$ and $PS_{266}$-*b*-$PMAPOSS_{20}$ lamellar morphologies (Figure 6a,c).

**Characterization of Hierarchical Structures in Thin Films Using GIWAXS Study.** As thermal annealing led to a second level of ordering within the PMAPOSS domain, we further examined the self-assembly in thin films by GIWAXS and AFM. GIWAXS is known to provide a high-intensity scattering

pattern with high statistical significance even for nanoscale thin films supported on substrates.[23] Previously, we had reported that solvent annealing in $CS_2$ is very effective in inducing vertical domain orientation in the PMAPOSS BCPs. We applied the same conditions to cylinder forming $PMMA_{41}$-*b*-$PMAPOSS_{29}$ with an additional thermal annealing step to further drive the POSS aggregation within the domains. The thin films were annealed in $CS_2$ for 10 h, followed by thermal annealing at 190 °C for 6 h under vacuum. The AFM phase images clearly show HEX PMMA cylinders oriented vertically to the film in both thermally unannealed (Figure 7a) and thermally annealed samples (Figure 7b). These results indicate that even though the vertical structures were obtained by solvent annealing (which might trap nonequilibrium structures) on unmodified substrates, subsequent thermal annealing does not change the orientation or morphology. The GIWAXS pattern of thermally unannealed sample (Figure 7c) shows three amorphous hollow rings at $2\theta_f = 3.20°$ (2.5 nm), 7.88° (1.0 nm), and 16.10° (0.49 nm) which can be attributed to an average distance between the main chains of PMAPOSS (Figure 7f), the average distance between the POSS cages in the PMAPOSS block (Figure 7e), and the average distance between $-COOCH_3$ groups of the PMMA segments, respectively (Figure 7e). Since these are amorphous hollow rings, there is no net orientation within the PMAPOSS segments. However, after thermal annealing a number of sharp and regular scattering spots (Figure 7d) appear over a wide range of scattering angles which is characteristic of a lattice structure. From indexing of the scattering spots in the 2D GIWAXS pattern (Figure 7d), the lattice structure was determined to be a orthorhombic unit cell with dimensions of 2.4 and 5.0 nm on the *y*- and *z*-axis directions, respectively. Figure 7f is a cartoon representation of the lattice structure of the PMAPOSS block as simulated by Cerius[2] software package. In thin films, the PMAPOSS block forms a helix-like structure to relieve the steric crowding of the POSS units. In the thermally unannealed sample, these helix-like structures are randomly oriented, whereas upon thermal annealing POSS aggregation drives the helical units to pack into an orthorhombic lattice. Upon annealing, the average distance between the PMMA cylinders changes from 32 to 27 nm (measured by AFM) and the size of the PMMA cylinder changes from 15 to 11 nm due to POSS aggregation. These results in thin films are consistent with the observations in bulk sample (Figure 6) where the appearance of diffraction peaks at 5.0 and 2.3 nm upon annealing shows the formation of orthorhombic unit cell by the aggregation of POSS units. The diffraction peak at 2.5 nm is a higher order peak of the peak at 5.0 nm.

**Conclusions.** We have demonstrated the living anionic polymerization of POSS-containing methacrylate monomer. The molecular weight increases linearly with the monomer/initiator ratio while maintaining a narrow polydispersity which confirms the living nature of the polymerization. Two kinds of BCPs, namely PMMA-*b*-PMAPOSS and PS-*b*-PMAPOSS, were synthesized. Both bulk samples and thin-film samples were characterized by TEM and synchrotron X-ray scattering. Because of the tunability of the PMAPOSS length by anionic polymerization, a rich range of morphologies such as spheres, cylinders, and lamellae were obtained for both sets of BCPs. In thin films, the PMAPOSS segments form a helix-like structure to relieve the steric crowding of the POSS units. Upon thermal annealing POSS aggregation drives the helical units to pack into an orthorhombic lattice structures. The excellent self-assembling characteristics in both bulk and thin films, good etch selectivity between the blocks, and access to a wide range of domain sizes and morphologies make these POSS-based BCPs an ideal candidate for BCP lithography.

**Acknowledgment.** T.H. acknowledges the Mitsubishi Chemical Corporation Fund. P.G. acknowledges the Medical School Electron Microscope Facility and Materials Science Center at University of Wisconsin, Madison. The authors acknowledge Dr. Li and Dr. Wang from Argonne National Laboratories for supporting the bulk X-ray diffraction studies and Prof. Tokita and Prof. Uchida from Tokyo Institute of Technology for the SEC MALS analysis. This work was partially supported by the UW-NSF Nanoscale Science and Engineering Center (DMR-0425880) and NSF-DMR CAREER 0449688. M.R. acknowledges the Ministry of Education, Science and Technology (MEST) (BK21 and World Class University Programs) and the Korea Research Foundation (National Research Laboratory for Polymer Synthesis and Physics and Center for Electro-Photo Behaviors in Advanced Molecular Systems). The synchrotron X-ray scattering measurements on thin films were supported by the MEST, POSCO, and Postech Foundation.

**Supporting Information Available:** SEC traces of the macroinitiator $PMMA_{262}$ and $PMMA_{262}$-*b*-$PMAPOSS_{23}$ (Figure S1); SEC traces of the macroinitiator $PS_{266}$ and $PS_{266}$-*b*-$PMAPOSS_{20}$ (Figure S2). This material is available free of charge via the Internet at http://pubs.acs.org.

## References and Notes

(1) Park, M.; Harrison, C.; Chailin, P. M.; Register, R. A.; Adamson, D. H. *Science* **1997**, *276*, 1401.
(2) (a) Kim, H.-C.; Jia, X.; Stafford, C. M.; Kim, D. H.; McCarthy, T. J.; Tuominen, M.; Hawker, C. J.; Russell, T. P. *Adv. Mater*. **2001**, *13*, 795. (b) Yoon, J.; Yang, S. Y.; Heo, K.; Lee, B.; Joo, W.; Kim, J. K.; Ree, M. *J. Appl. Crystallogr*. **2007**, *40*, 305. (c) Yang, S. Y.; Park, J.; Yoon, J.; Ree, M.; Jang, S. K.; Kim, J. K. *Adv. Funct. Mater*. **2008**, *18*, 1371.
(3) Thurn-Albrecht, T.; Steiner, R.; DeRouchey, J.; Stafford, C. M.; Huang, E.; Bal, M.; Tuominen, M.; Hawker, C. J.; Russell, T. P. *Adv. Mater*. **2000**, *12*, 787.
(4) Park, S.; Wang, J.-Y.; Kim, B.; Russell, T. P. *Nano Lett*. **2008**, *8*, 1667.
(5) Olayo-Valles, R.; Guo, S.; Lund, M. S.; Leighton, C.; Hillmyer, M. A. *Macromolecules* **2005**, *38*, 10101.
(6) Park, S.; Lee, D. H.; Xu, J.; Kim, B.; Hong, S. W.; Jeong, U.; Xu, T.; Russell, T. P. *Science* **2009**, *323*, 1030.
(7) Lammertink, R. G. H.; Hempenius, M. A.; van den Enk, J. E.; Chan, V. Z.-H.; Thomas, E. L.; Vancso, G. J. *Adv. Mater*. **2000**, *12*, 98.
(8) Lu, J.; Chamberlin, D.; Rider, D. A.; Liu, M.; Manners, I.; Russell, T. P. *Nanotechnology* **2006**, *17*, 5792.
(9) Fukukawa, K.; Zhu, L.; Gopalan, P.; Ueda, M.; Yang, S. *Macromolecules* **2005**, *38*, 263.
(10) Jung, Y. S.; Ross, C. A. *Nano Lett*. **2007**, *7*, 2046.
(11) Stoykovich, M. P.; Nealey, P. F. *Mater. Today* **2006**, *9*, 20.
(12) Tegou, E.; Bellas, V.; Gogolides, E.; Argitis, P.; Eon, D.; Cartry, G.; Cardinaud, C. *Chem. Mater*. **2004**, *16*, 2567.
(13) Haddad, T. S.; Lichtenhan, J. D. *Macromolecules* **1996**, *29*, 7302.
(14) Zheng, L.; Waddon, A. J.; Farris, R. J.; Coughlin, E. B. *Macromolecules* **2002**, *35*, 2375.
(15) Zheng, L.; Hong, S.; Cardoen, G.; Burgaz, E.; Gido, S. P.; Coughlin, E. B. *Macromolecules* **2004**, *37*, 8606.
(16) Pyun, J.; Matyjaszewski, K.; Wu, J.; kim, G. -M.; Chun, S. B.; Mather, P. T. *Polymer* **2003**, *44*, 2739.
(17) Hayakawa, T.; Seino, M.; Goseki, R.; Hirai, T.; Kikuchi, R.; Kakimoto, M.; Tokita, M.; Yokoyama, H.; Horiuchi, S. *Polym. J*. **2006**, *38*, 567.
(18) Hirai, T.; Leolukman, M.; Hayakawa, T.; Kakimoto, M.; Gopalan, P. *Macromolecules* **2008**, *41*, 4558.

(19) Hirai, T.; Leolukman, M.; Liu, C. C.; Han, E.; Kim, Y. J.; Ishida, Y.; Hayakawa, T.; Kakimoto, M.; Nealey, P. F.; Gopalan, P. *Adv. Mater.*, in press.
(20) (a) Ree, M.; Ko, I. S. *Phys. High Tech.* **2005**, *14*, 2. (b) Yoon, J.; Kim, K.-W.; Kim, J.; Heo, K.; Jin, S.; Shin, T. J.; Lee, B.; Rho, Y.; Ahn, B.; Ree, M. *Macromol. Res.* **2008**, *16*, 575.
(21) Varshney, S. K.; Hautekeer, J. P.; Fayt, R.; Jérôme, R. Teyssié, Ph. *Macromolecules* **1990**, *23*, 2618.
(22) Maeda, R.; Hayakawa, T.; Tokita, M.; Kikuchi, R.; Kouki, J.; Kakimoto, M.; Urushibata, H. *React. Funct. Polym.* **2009**, *69*, 519.
(23) (a) Lee, B.; Park, Y.-H.; Hwang, Y.-T.; Oh, W.; Yoon, J.; Ree, M. *Nat. Mater.* **2005**, *4*, 147. (b) Lee, B.; Oh, W.; Hwang, Y.; Park, Y.-H.; Yoon, J.; Jin, K. S.; Heo, K.; Kim, J.; Kim, K.-W.; Ree, M. *Adv. Mater.* **2005**, *17*, 696. (c) Lee, B.; Yoon, J.; Oh, W.; Hwang, Y.; Heo, K.; Jin, K. S.; Kim, J.; Kim, K.-W.; Ree, M. *Macromolecules* **2005**, *38*, 3395. (d) Lee, B.; Park, I.; Yoon, J.; Park, S.; Kim, J.; Kim, K.-W.; Chang, T.; Ree, M. *Macromolecules* **2005**, *38*, 4311. (e) Jin, S.; Yoon, J.; Heo, K.; Park, H.-W.; Shin, T. J.; Chung, B.; Chang, T.; Ree, M. *J. Appl. Crystallogr.* **2007**, *40*, 950. (f) Yoon, J.; Jin, S.; Ahn, B.; Rho, Y.; Hirai, T.; Maeda, R.; Hayakawa, T.; Kim, J.; Kim, K.-W.; Ree, M. *Macromolecules* **2008**, *41*, 8778.